Human Eyeball Model Reconstruction and Quantitative Analysis

Qi Xing and Qi Wei

Abstract— **Determining shape of the eyeball is important to diagnose eyeball disease like myopia. In this paper, we present an automatic approach to precisely reconstruct three dimensional geometric shape of eyeball from MR Images. The model development pipeline involved image segmentation, registration, B-Spline surface fitting and subdivision surface fitting, neither of which required manual interaction. From the high resolution resultant models, geometric characteristics of the eyeball can be accurately quantified and analyzed. In addition to the eight metrics commonly used by existing studies, we proposed two novel metrics, Gaussian Curvature Analysis and Sphere Distance Deviation, to quantify the cornea shape and the whole eyeball surface respectively. The experiment results showed that the reconstructed eyeball models accurately represent the complex morphology of the eye. The ten metrics parameterize the eyeball among different subjects, which can potentially be used for eye disease diagnosis.**

I. Introduction

Eyeball size and geometric features provide valuable information on certain type of vision disorders. For instance, positive correlation between the axial length of the eyeball and the degree of myopia has been found through quantitative analysis [1, 2]. Various eyeball geometric characteristics have been represented by different methods in both two dimensions (2D) [3-5] and more recently in three dimensions (3D) [6-8]. Previous studies have used Magnetic Resonance Imaging (MRI) to quantify the size and shape of eyeball. Curvatures of the retinal surfaces were analyzed [3, 6], and 3D eyeball models were built [7, 8]. Previous analysis required manual effort on image processing and model reconstruction, which were labor expensive and may introduce user dependent artifacts. In addition, there are many other clinically important questions regarding the eyeball surface features that have not been investigated, such as the statistical variations of the eye shape of a large population and the possible gaze-dependent eye shape changes of normal subjects. These questions demand accurate, robust and efficient computational algorithms to build 3D models from medical images.

To address the limitation of existing approaches that measure the geometric characteristics of eyeball, in this paper, we develop a new method to reconstruct detailed 3D models of the eyeballs from T2-weighted MR images. Our goal is that this automatic modeling framework can be used on analyzing large datasets and generalized to data with different kinds of pathologies. The generated models can help to (1) understand scientific questions such as whether eyeball deforms as a function of gaze and (2) assist clinicians for diagnosis. Parametric geometric representation is used, which has the advantage of continuity and smoothness. We propose to characterize eyeball shape by ten characteristic metrics. Our reconstruction approach and quantitative methods will be useful for eye disease diagnosis benefiting by the accurate eyeball shape representation and comprehensive description by the ten metrics. This paper is organized as follows. In Section II, we present several approaches developed to build 3D eyeball model. In section III, we describe how to establish the local coordinate system of each eye ball (LCS) and introduce ten geometric metrics used to quantify eyeball shape. Results are presented in Section IV, followed by conclusion in Section V.

Qi Xing is with the Department of Computer Science, George Mason University, 4400 University Drive, Fairfax, VA 22030, USA. (e-mail: qxing@gmu.edu).

Qi Wei is with the Department of Bioengineering, George Mason University, 4400 University Drive, Fairfax, VA 22030, USA. (phone: 703-993-5211; e-mail: qwei2@gmu.edu).

II. Method

Our template-based eyeball shape reconstruction approach is outlined in Algorithm 1, the details of which are presented in the following.

Algorithm 1: Template-based Eyeball Reconstruction

1. Segment eyeball boundaries B_c from coronal MR images
2. Segment eyeball boundaries B_s from sagittal MR images (Section II.A.)
3. Register edge points to using ICP variant: $B_c \rightarrow B_c'$ (Section II.B.)
4. Fit a B-Spline surface $S_{BSpline}$ to $B_c \cap B_s$ which are sparse in space
5. Fit a subdivision surface S_{subdiv} to densely sampled vertices P from $S_{BSpline}$(Section II.C.)

A. Image Segmentation

Compared to T1-weighted MRI, T2-weighted MRI provides excellent contrast between the eyeball and its surrounding tissues and hence enables automated boundary segmentation. Our segmentation method is described in Fig. 1. The original images in the sagittal view (Fig. 1(a)) and coronal view (Fig. 1(d)) were first preprocessed by a Gaussian filter. The Canny edge detection method [9] was then applied to extract the structure boundaries with the specified Canny sensitivity thresholds [0.06 0.15] (Fig. 1(b) and 1(e)). As can be seen from Fig. 1(b), edge detection outputted undesired landmarks inside the eyeball. Therefore, we used Deformable Snake to determine the eyeball boundaries, the points on which were denoted by *Bs* and *Bc* respectively, from coronal and sagittal MR images (Fig. 1 (c) and 1(f)).

B. Boundary Registration

Registration between the two boundary sets, *Bs* and *Bc*, was performed to correct movement of the subject between acquisition of the sagittal images and the coronal images. We used a variant of the iterative closet point (ICP) [10] algorithm to find the best alignment between *Bs* and *Bc* (Fig. 1 (c)(f)).

978-1-4244-7929-0/14/$26.00 ©2014 IEEE

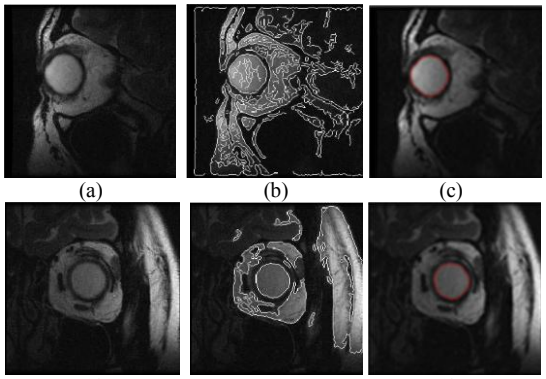

Figure 1. MRI image segmentation. (a)(c) Images resulted from application of Gaussian filter; (b)(d) Canny edge detection was applied to all images to extract landmarks; (e)(f) Eyeball boundaries were determined from Deformable Snake method.

Neither Bc nor Bs completely sampled the whole eyeball geometry because of the difficulty in accurately segmenting images near the poles of the eyeball. In addition, Bs and Bc are from a nearly spherical structure which may lead to ambiguous registration. To avoid such false correspondence, for each data point on one boundary, we only searched for its closest point on the other boundary that was within a predetermined distance. This was a fair constraint applied since movement of the subject between scans was expected to be small. A rigid transformation was computed which translated and rotated one set of boundary points to the other set. Fig. 2 shows registration results. ICP algorithm was applied to Bs (red) and Bc (blue). Subject movement was optimally eliminated which transformed the coronal boundaries to the new locations Bc' (showed by the magenta points), providing a more accurate representation of the eyeball shape.

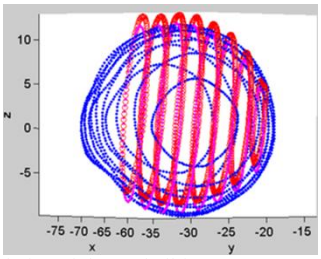

Figure 2. Boundaries of the eyeball in two scans were registered to correct displacement between scans.

C. *Eyeball Reconstruction*

A two-step surface fitting process was developed to realistically model the complete shape of the eyeball from the extracted boundaries. First, a B-Spline surface [11] was fitted to all the boundaries points using an approach previously developed [12]. The fitted B-Spline surface closely modeled the overall geometry of the eyeball (see Fig. 3(a)). However, since we used a B-Spline surface with opening endings, artifacts occurred at two ends. Achieving mesh uniformness on B-spline surfaces is important for shape analysis and is not straightforward. Therefore, we employed the Loop's subdivision surface [13] to refine the B-Spline surface. Algorithm 2 describes our approach on fitting a subdivision surface S_{subdiv} to the vertices P on the B-Spline surface.

Algorithm 2: Subdivision Surface Fitting

```
1.  for each iteration do
2.      for each vertex v_i on S_subdiv do
3.          find v_i' three closest vertices in P: p1, p2, and p3
4.          Compute v_i'projection v_i on the plane formed by p1, p2, and p3
5.          v_i ← v_i
6.      end for
7.  perform mesh smoothing on S_subdiv
8.  end for
```

Fig. 3(b) and (c) shows the reconstructed and refined eyeball geometry fitted to the boundary points in Fig. 3(a). The fitting error of this example, defined as the mean distance from the boundary points to the resultant B-Spline surface, was 0.0007 mm. The subdivision fitting error, defined as the mean distance from the vertices on the subdivision surface to the B-Spline surface, was 0.05mm. Both fitting errors were reasonably small, which demonstrates that the resultant subdivision surface closely represent the geometric shape of the eyeball.

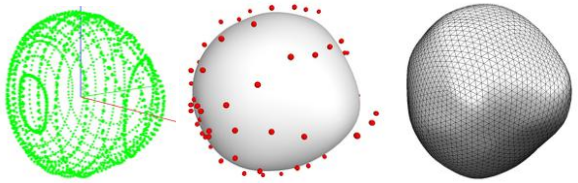

Figure 3. (b) A B-Spline surface was fitted to (a) the original boundary points which were segmented from the MRI images in Fig. 1. (c) A subdivision surface was fitted to (b) the B-Spline surface.

III. Eyeball Quantitative and Evaluation

Based on the reconstructed eyeball surfaces, for the first time, we apply Gaussian curvature [14] as a new metric to analyze shape of the cornea surface. Using Gaussian curvature and geometric relationship between the left and right eyeballs, the local coordinate system (LCS) for each eyeball can be created as the standardized coordinate system to better describe the topology features of the eyeball. With subject-specific LCS established, eight other metrics (surface area, volume, LCS axial length (Axial L), LCS horizontal length (Horiz L), LCS vertical length (Vert L), ellipsoid axial length (Axial L), ellipsoid horizontal length (Horiz L), and ellipsoid vertical length (Vert L) can be computed to parameterize and quantify the geometric features of the eyeball in 3D. Some of these metrics have been used in previous work [7, 8] and here we propose a more comprehensive set of features. The tenth metric is the eyeball Sphere Distance Deviation (SDD), measuring the deviation of the eyeball to the sphere that best approximate it. We will introduce how these metrics were calculated from the 3D models.

A. *Cornea Feature Analysis using Gaussian Curvature*

In computational geometry, the Gaussian curvature of a point on the surface is the product of the principal curvatures at that point [14]. The principal curvatures are the normal curvatures, which measure the maximum and minimum

blending of the surface at each point. The tangent plane of a point with positive Gaussian curvature intersects the surface at a single point, whereas the tangent plane of a point with negative Gaussian curvature cuts through the surface [15]. Therefore, the Gaussian curvature determines whether a surface is locally convex or locally concave. If the Gaussian curvature is positive (negative), then the surface at that point is convex (concave). The actual curvature value other than the sign quantitatively implies the degree of convexity (concavity) at any point on a surface. Fig. 4(a) illustrates the Gaussian curvature on the two eyeball surface of one subject. The Gaussian curvature is relatively high near the cornea (red) and low near the ciliary body (blue). This metric can be used to show the shape characteristics of myopia and highly myopia, since it has been suggested that myopia is associated with deformation of the cornea [8]. Such deformation might stretch the cornea along the axial direction which leads to more extrusive cornea shape accompanied by a more concave transition between cornea and sclera.

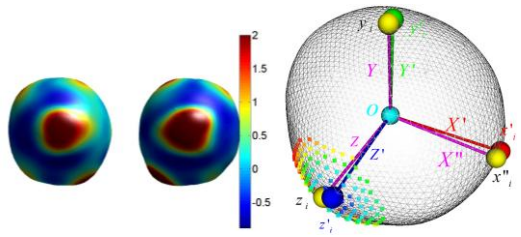

(a) (b)

Figure 4. Cornea Feature Analysis using Gaussian Curvature. (a) Gaussian Curvature; (b) LCS of an eyeball

B. Local Coordinate System (LCS)

As stated above, forming a local coordinate system is the key to better parameterize features of the eyeball surface. In this section, we describe how the LCS can be established for each eyeball. First, geometric center o of the eyeball surface (shown as the cyan ball in Fig. 4 (b)) was calculated, and the global coordinate system $(o: X, Y, Z)$ was initialized at o. The intersection point Z_i (yellow ball) of the Z-axis (magenta axis) and the eyeball surface was close to the center of the cornea because of how the MRI scan was oriented. Since the calculated Gaussian curvature quantifies local geometric characteristics of the cornea surface, we applied k-nearest search algorithm [16] at point Z_i to find the region on cornea surface that had the highest Gaussian curvature (see small blue dots on eyeball surface in Fig.4 (b)). Then arithmetic mean of the region was computed to obtain a new center of cornea Z_i' (blue ball). By connecting o and Z_i', a new Z' axis was generated (blue axis in Fig. 4(b)).

Second, we followed Singh et al.'s method [7] to create the initial X"-axis (magenta axis) by forming a line that goes through the left and right eyeballs' geometric center. Notice that we could not guarantee that X" is perpendicular to Z', so further adjustment was needed.

Finally, the cross product between Z' and X" formed the new axis Y' (green axis). The new X' axis (red axis) was calculated through the cross product of the Y' and Z'. The resultant LCS $(o: X', Y', Z')$ was shown in Fig. 4(b).

C. Sphere Fitting of the Eyeball

The geometric shape of an emmetropic eye is close to being spherical in 3D whereas an abnormal eye such as myopia and highly myopia shows deformation or distortion from a sphere [8]. Moriyama et al. introduced a new metric that classified the highly myopic eyes into four basic types on the 3D reconstructed eyeball surface [8]. But this classification procedure can only be performed based on the experienced professionals' judgment to manually analyze each eye and their agreement on the classification results. This time-consuming process is subjected to human error. In addition, the topologic features of the eye can hardly be measured using the approach in [8], making it difficult to describe the topologic difference between the emmetropic and abnormal eyes. To overcome this problem, we applied the RANSAC algorithm [17] to fit eyeball surface by a sphere and measure the Sphere Distance Deviation (SSD) between the surface and the sphere. The main steps were outlined in Algorithm 3.

Algorithm 3: Fitting a Sphere to the eyeball subdivision surface

1. Sample the eyeball surface and output a point cloud
2. Apply RANSAC algorithm to fit a spherical surface to the point cloud
3. Compute the SSD between the eyeball surface to the sphere surface

Fig. 5(a) illustrates the sphere fitting result that closely approximated the eyeball. We define the SSD Δd, which measures distance between the eyeball and the sphere, as:

$$\Delta d(p_i) = d(p_i) - r, i = 0 \ldots n \quad (1)$$

where p_i is a vertex on the eyeball surface, $d(p_i)$ is the distance from p_i to the fitted sphere center and r is the radius of the fitted sphere. $\Delta d(p_i)$ is positive if p_i is outside the sphere, and $\Delta d(p_i)$ is negative if p_i is inside the sphere, which means eyeball surface at point p_i intersects with the sphere. When $\Delta d(p_i) = 0$, p_i is on the sphere surface. To better represent the SSD, the $\Delta d(p_i)$ is normalized between 0 and 1. Fig. 5(b) shows histogram of the normalized $\Delta d(p_i)$, and Fig. 5(c) illustrates the colored sphere that maps $\Delta d(p_i)$ on the fitted sphere surface.

IV. Result

Table 1 summarizes the quantitative results for twenty eyeballs reconstructed from MRI of ten healthy subjects, who were identified only by their two-letter IDs. Anonymous MRI data was provided by Dr. Joseph Demer at UCLA.

According to the table, the mean Axial, Horizontal (Horiz) and Vertical (Vert) Length (L) in the local coordinate system are almost the same. The mean ± standard deviation of SSD is 0.005(±0.05) mm, showing that the fitted sphere can closely approximate the eyeball surface and measure spherical deviation.

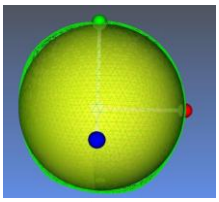

(a)

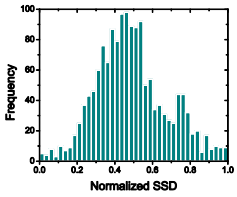

(b)

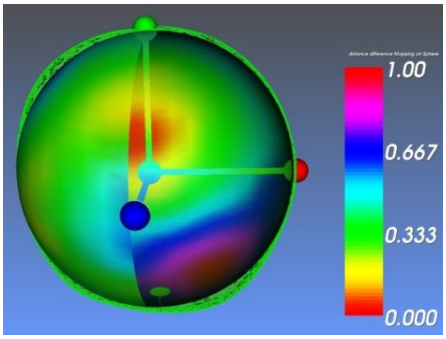

(c)

Figure 5. Analysis of the eyeball's deviation from a sphere. (a) Eyeball and fitted sphere; (b) Histogram of computed SSD; (c) Color mapped SSD

TABLE I. EYEBALL QUANTITATIVE RESUTLS

		Mean	SD
Surface Area (mm^2)		1673.60	151.52
Volume (mm^3)		6395.31	877.62
LCS	**Axial L (mm)**	23.20	1.14
	Horiz L (mm)	23.33	0.93
	Vert L (mm)	23.85	1.24
Ellipsoid	**Axial L (mm)**	21.94	1.06
	Horiz L (mm)	23.12	0.95
	Vert L (mm)	23.56	1.28
SSD (mm)		0.005	0.05

V. CONCLUSION

We have developed a computational framework for building subject-specific eye model from MRI, using parametric surface fitting. 3D eyeball geometric models from difference subjects can be accurately and efficiently reconstructed. Analysis results are consistent with previous studies [6-8]. Moreover, our approach provided comprehensive quantitative analysis of ocular anatomy and morphology by using the eight basic metrics. We proposed two more metrics, the Gaussian curvature and the sphere distance deviation, that have not been utilized previously but could improve the accuracy and efficiency of the diagnosis of the vision disorders. In the future, we will apply the approach on more datasets and aim to find the correlation between refractive error and shape feature, which can then be used for clinical diagnosis.

ACKNOWLEDGMENT

We would like to thank Dr. Joseph Demer for proving anonymous MRI data and valuable suggestions. We would also like to thank Dr. Dinesh Pai for discussions on surface fitting. The study was supported by a George Mason University faculty startup grant and a seed Research Award to Dr. Wei.

REFERENCES

[1] S.-W. Cheung and P. Cho, Validity of Axial Length Measurements for Monitoring Myopic Progression in Orthokeratology, *Investigative Ophthalmology & Visual Science*, Vol. 54(3), pp. 1613–1615, 2013.

[2] L. Llorente, S. Barbero, D. Cano, C. Dorronsoro, and S. Marcos, Myopic Versus Hyperopic Eyes: Axial Length, Corneal Shape and Optical Aberrations, *Journal of Vision*, Vol. 4(4), pp. 288-298, 2004.

[3] D. O. Mutti, J. R Investigative Ophthalmology & Visual Science. Hayes, G. L. Mitchell, L. A. Jones, M. L. Moeschberger, S. A. Cotter, R. N. Kleinstein, R. E. Manny, J. D. Twelker, K. Zadnik, and CLEERE Study Group, Refractive Error, Axial Length, and Relative Peripheral Refractive Error before and after the Onset of Myopia, *Investigative Ophthalmology & Visual Science*, Vol. 48(6), pp. 2510–2519, 2007.

[4] D. A. Atchison, C. E. Jones, K. L. Schmid, N. Pritchard, J. M. Pope, W. E. Strugnell, and R. A. Riley, Eye Shape in Emmetropia and Myopia, *Investigative Ophthalmology & Visual Science*, Vol. 45(10), pp. 3380–3386, 2004.

[5] K. Ishii, H. Iwata, and T. Oshika, Quantitative Evaluation of Changes in Eyeball Shape in Emmetropization and Myopic Changes Based on Elliptic Fourier Descriptors, *Investigative Ophthalmology & Visual Science,* Vol. 52(12), pp. 8585–8591, 2011.

[6] D. A. Atchison, N. Pritchard, K. L. Schmid, D. H. Scott, C. E. Jones, and J. M. Pope, Shape of the Retinal Surface in Emmetropia and Myopia, *Investigative Ophthalmology & Visual Science*, Vol. 46(8), pp. 2698–2707, 2005.

[7] K. D. Singh, N. S. Logan, and B. Gilmartin, Three-dimensional Modeling of the Human Eye based on Magnetic Resonance Imaging, *Investigative Ophthalmology & Visual Science*, Vol. 47(6), pp. 2272–2279, 2006.

[8] M. Moriyama, K. Ohno-Matsui, K. Hayashi, N. Shimada, T. Yoshida, T. Tokoro, and I. Morita, Topographic Analyses of Shape of Eyes with Pathologic Myopia by High-resolution Three-dimensional Magnetic Resonance Imaging, *Ophthalmology*, Vol. 118(8), pp. 1626–1637, 2011.

[9] J. Canny, A Computational Approach to Edge Detection, *IEEE Transaction on Pattern Analysis and Machine Intelligence*, Vol. 8(6), pp. 679–698, 1986.

[10] Z. Zhang, Iterative Point Matching for Registration of Free-form Curves, *International Journal of Computer Vision,* Vol. 13(2), pp.119-152, 1992.

[11] M. Eck, Automatic Reconstruction of B-spline Surfaces of Arbitrary Topological Type, *SIGGRAPH'96*, pp. 325–334, 1996.

[12] Q. Wei and D.K. Pai, Physically Consistent Registration of Extraocular Muscle Models from MRI, *Engineering in Medicine and Biology Society 2008 (EMBC08),* pp. 2237-2241.

[13] C. T. Loop, Smooth Subdivision Surfaces based on Triangles, M.S. dissertation, Department of Mathematics, University of Utah, 1987.

[14] I. R. Porteous, *Geometric Differentiation: For the Intelligence of Curves and Surfaces*. New York: Cambridge University Press, 2001.

[15] W. Kuhnel and B. Hunt, *Differential Geometry: Curves - Surfaces - Manifolds*. American Mathematical Society, 2006.

[16] T. Cover and P. Hart, Nearest Neighbor Pattern Classification, *IEEE Transaction on Information Theory*, Vol. 13(1), pp. 21–27, 1967.

[17] M. A. Fischler and R. C. Bolles, Random Sample Consensus: A Paradigm for Model Fitting with Applications to Image Analysis and Automated Cartography, *Communication of the ACM*, vol. 24(6), pp. 381–395, 1981.